EUROPEAN COMMISSION

HORIZON 2020 PROGRAMME - TOPIC H2020-LC-BAT-2020
Sodium-Ion and sodium Metal BAtteries for efficient and sustainable next-generation energy storage

GRANT AGREEMENT No. 963542

SIMBA – Deliverable Report

<< D3.3 – Quantification of Na^+ transfer at electrode/electrolyte interfaces >>

Deliverable No.	SIMBA D3.3	
Related WP	WP3	
Deliverable Title	Quantification of Na^+ transfer at electrode/electrolyte interfaces	
Deliverable Date	2021-12-31	
Deliverable Type	REPORT	
Dissemination level	Public (PU)	
Written By	Magdalena Graczyk-Zajac (TUDa)	2021-12-12
Checked by	Ying Zhan (TUDa)	2021-12-13
Reviewed by (if applicable)	Pavol Šajgalík (SAS)	2021-12-16
Approved by	Ralf Riedel (TUDa)	2021-12-20
Status	Final	2021-12-20

This project has received funding from the European Union's Horizon 2020 research and innovation programme under grant agreement No 963542.

Publishable summary

A deep understanding of the interaction between the solid-state electrolyte and the electrodes is essential for the development of an efficient all-solid-state battery. Stable interfaces with the anode and cathode will ensure inherent safety and will ultimately lead to the extended lifetime of the battery. Highly efficient electrolyte/electrode interfaces through an intimate solid-solid contact are a key feature of solid-state batteries. One of the key challenges toward high-performance solid-state batteries is the large impedance posed by the electrode-electrolyte interface. However, a direct assessment of the charge transport across realistic electrode-electrolyte interfaces is tedious. The lack of understanding of the processes at the interfaces between the electrolyte and the electrodes is one of the biggest challenges for sodium ion batteries.

In this report we list and discuss in detail the possible ways of the evaluation of the diffusion coefficients of sodium in the electrode (both cathode and anode), electrolyte and well as the charge transfer resistances across the electrode/electrolyte interface. This description provides a “mode d’emploi” (detailed guideline) on how to determine a charge transfer across the cathode/electrolyte interface. Accordingly, the methodology of experimental and modelling approaches allowing to assess the charge transfer properties of the interface is addressed in line with the limits of the technique. The detailed description of the evaluation of the sodium ion transfer in the interface using NMR spectroscopy and single particle measurements is presented in line with a determination of sodium transport using molecular dynamic simulation and DFT calculations. Summarizing, here we aim to provide a trend-setting toolbox allowing to characterize and to improve the charge transfer/ion mobility in the electrode/electrolyte interface.

Please keep in mind that a detailed didactic description of a methodology proposed in this document in line with scientific basics for the discussed techniques has been presented in Deliverable 3.1 and 3.2 and is not in the focus of a present deliverable.

Contents

1 Purpose of the document 5
1.1 Document structure 5
1.2 Deviations from original description in the Grant Agreement Annex 1 Part A 5
1.2.1 Descriptions of work related to deliverable in GA Annex 1 – Part A 5
1.2.2 Time deviations from original planning in GA Annex 1 – Part A 5
1.2.3 Content deviations from original plan in GA Annex 1 – Part A 5
2 Introduction 6
3 Evaluation of the Na^+ transfer using NMR spectroscopy 7
4 Evaluation of sodium transport via modelling 9
5 Evaluation of the Na^+ transfer using single particle measurements 10
6 Conclusions and Recommendations 12
7 Risk Register 13
8 References 14
Appendix A - Table of Abbreviations 15
Appendix B - Acknowledgement 16
Appendix C - Disclaimer/Acknowledgement 17

Figures

Figure 1: Schematic representation of the all-solid-state battery (adapted from [1]). 6
Figure 2: Schematic representation of the cathode/solid electrolyte interfaces, adopted from http://smeng.ucsd.edu/supercapacitors/ 7
Figure 3: Single-phase disordered (hard) carbon; model construction 9
Figure 4: Rate capability for SiCN-1300 at 60 °C. 10
Figure 5: Tafel plot of HN3-1300 at 60 °C and DOD=10 %. 10
Figure 6: Tafel plot of SiCN-1300 at RT and DOD=10 %. 11
Figure 7: SEM micrograph of a single particle 11

1 Purpose of the document

This document corresponds to D3.3 – Quantification of Na^+ transfer at electrode/electrolyte interfaces. The ways of the evaluation of the diffusion coefficients of sodium in the electrode, electrolyte and well as the charge transfer resistances across the electrode/electrolyte interface will be introduced in this deliverable report as a guidebook for the SIMBA research. This description provides a "mode d'emploi" (detailed guideline) on how to determine a charge transfer across the cathode/electrolyte interface.

1.1 Document structure

This document consists of four main parts:

Chapter 2 Introduction

Chapter 3 Evaluation of the Na+ transfer using NMR spectroscopy

Chapter 4 Estimation of sodium transport via modelling

Chapter 5 Evaluation of the Na^+ transfer using single particle measurements

1.2 Deviations from original description in the Grant Agreement Annex 1 Part A

1.2.1 Descriptions of work related to deliverable in GA Annex 1 – Part A

N/A.

1.2.2 Time deviations from original planning in GA Annex 1 – Part A

N/A.

1.2.3 Content deviations from original plan in GA Annex 1 – Part A

N/A.

2 Introduction

All-solid-state batteries (ASSB) with nonflammable solid electrolytes (SE) experience fast-growing interest. Apart from enhanced safety, ASSB can offer longer cycle life, higher energy density, fewer requirements on packaging and state-of-charge monitoring circuits, when compared to liquid-electrolyte based batteries [2-4].

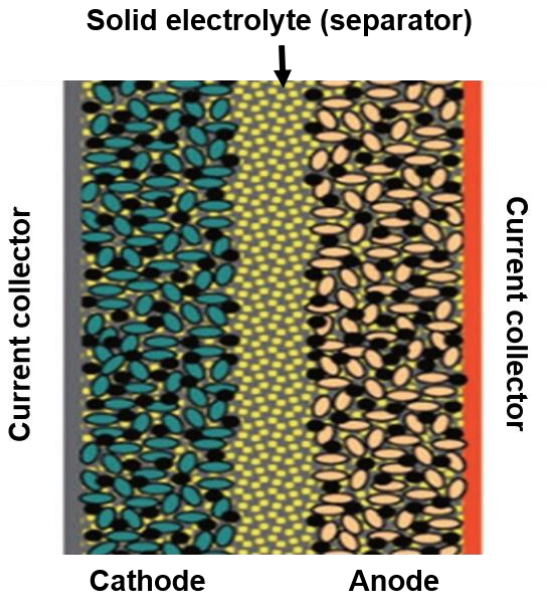

Figure 1: Schematic representation of the all-solid-state battery (adapted from [1]).

The all-solid-state battery consists of a solid cathode, electrolyte and anode (Figure 1). The solid electrolyte plays a critical role functioning as both an ionic conductor and separator and should possess high ionic conductivity and negligible electronic conductivity, a wide voltage window and chemical compatibility with the electrodes. It should also be simple to fabricate on a large scale at a low cost. Besides the intrinsic ionic conductivity of the solid electrolyte, the electrode/electrolyte interface defines the ohmic losses of the cell and, ultimately, the overall cell performance. The high interfacial resistance is therefore considered as one of the major drawbacks hindering the commercialization of all-solid-state secondary batteries [4-7]. Clearly, the bottleneck of ASSB development is no longer maximizing the ionic conductivity of solid electrolytes but has instead shifted towards establishing intimate electrode-electrolyte contacts [8]. The impedance induced by the lack of contacts arises from various imperfections at the solid electrolyte/electrode interface [5, 9-11]. Surface modifications with ball-milling, coating and softening glassing have proved to be effective approaches to improve the charge transfer across the interfaces [12-14].

Nevertheless, it still represents a challenge to quantitatively assess the charge transfer properties across the interface. Figure 2 depicts a schematic representation of the cathode/solid electrolyte interface. The applied compaction pressure significantly affects the electrochemical performance of the composite.

Electrochemical impedance spectroscopy (EIS) is often used to characterize the charge transfer resistance. However, it is not always possible to clearly distinguish the interface from the bulk contribution. Experiments performed on single particles allow for avoiding the influence of the binder and conducting materials. So far, mostly electrochemical measurements of the active materials as "powder coated electrodes" have been presented. However, these electrodes possess a high fraction of additives, namely Carbon Black Super P® conductive additive and PVDF insulating binder, influencing the performance of the electrodes. Moreover, the composition, the porosity and the thickness of the electrodes can have a significant impact on the obtained results. Yet, it is of great interest to gain insight into the intrinsic properties of the active material. For this reason and in order to get a better resolution of the measurement, EIS and galvanostatic cycling might be applied on single material particles providing insights into the intrinsic nature of the charge transport.

Nuclear magnetic resonance (NMR) spectroscopy has been shown to offer unique complementary information to impedance spectroscopy, by its high sensitivity towards the lithium-ion mobility in battery materials [5, 10]. ^{7}Li NMR was proved to be a powerful tool to ascertain not only structural

features, but also dynamical properties of solid lithium-ion conductors [15]. The latter approach exploits that, in general, the ^{7}Li spins show different NMR frequencies ω when the corresponding lithium ions reside at distinguishable lithium sites since the NMR interactions are different in diverse local environments. Consequently, the time dependence of ω results from ionic jumps between various lithium sites. Several ^{7}Li NMR techniques are capable of probing this time dependence [15] and might be well applied for ^{23}Na studies. As various techniques operate in different time windows, a combination allows one to observe lithium ionic motion in a broad dynamic range. This approach is particularly useful in ^{7}Li NMR studies on disordered solids featuring strongly heterogeneous ion dynamics and is planned to be adopted in studies on sodium [15-22].

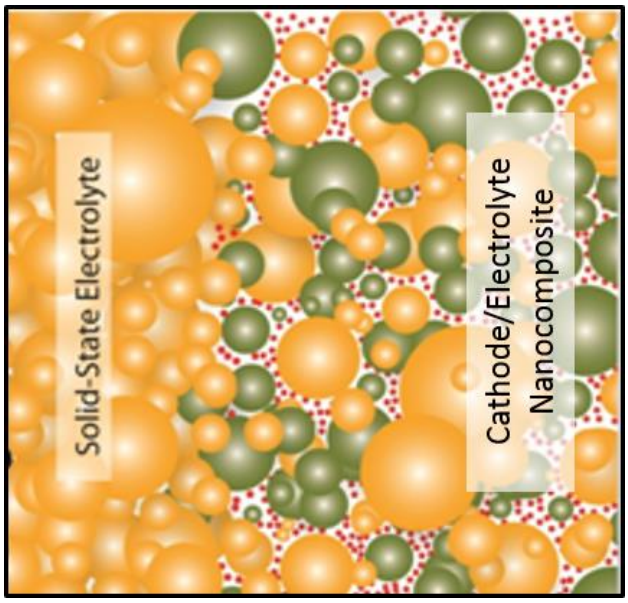

Figure 2: Schematic representation of the cathode/solid electrolyte interfaces, adopted from http://smeng.ucsd.edu/supercapacitors/

3 Evaluation of the Na^+ transfer using NMR spectroscopy

The neat electrode materials and mixtures of electrode/solid electrolyte materials, before and after cycling with varying sodium concentrations will be investigated. A multinuclear (^{13}C, ^{23}Na, ^{29}Si), field-dependent (14 T, 9.4 T, 7 T) variable temperature (VT, typically between 243 and 343 K) SSNMR spectroscopy to characterize the ^{23}Na-ions and their local environments as a function of the intercalated sodium will be applied. High resolution ^{23}Na-SSNMR experiments (MAS and 3QMAS) at high spinning speed (20 kHz) will be realized to provide chemical shifts and quadrupolar interactions in the electrolytes and the electrode materials. We will extend this method to ^{23}Na 1D VT-line-shape analysis and 2D NMR exchange experiments to monitor the ion mobility and extract the ion hopping rates, once electrode and electrolyte signals are clearly distinguished on the basis of chemical shift or quadrupolar interaction. Following, the sodium environment under electrochemical charge/discharge conditions will be monitored in the in-situ setup (please compare deliverable D3.2). We will investigate the effect of electric currents, temperature and the charging state on the distribution of sodium sites directly inside the probe by ^{23}Na-SSNMR. The effective diffusion coefficient (D_{eff}) of sodium during charging and recharging will be derived from ^{23}Na line-shape analysis and via chemical exchange NMR.

Furthermore, a combination of spin-lattice relaxation (SLR), line-shape analysis (LSA), and stimulated-echo experiments (STE) to determine correlation times in wide temperature and dynamic ranges might be used for the determination of the transport properties, using the following approach:

^{23}Na NMR spectra will be obtained from Fourier transformation of time signals following the solid-echo sequence. At low temperatures and slow lithium ionic motion, the diverse environments of the lithium ions cause broad static spectra with typical line widths Δω in the kHz regime. When the temperature is increased and cation jumps become faster, the spectra start to narrow as soon as the jump rate becomes comparable to the static line width Δω [15]. Thus, ^{23}Na LSA is sensitive to ion dynamics in the microsecond regime. Here, the temperature-dependent linewidth will be determined to obtain insights into such dynamics. Detailed information about cation jumps in the millisecond time range is available from ^{23}Na STE. This approach uses the stimulated-echo three-

pulse sequence, $90°_x$ - t_p – $45°_y$ - t_m – $45°_y$ - t_p, to correlate the NMR frequencies and, thus, the ionic positions during two short evolution times t_p, which are separated by a longer mixing time t_m. Specifically, the ^{23}Na STE technique provides access to the correlation function [22].

$$F_2(t_m) \propto \langle \sin[\omega(0)t_p] \sin[\omega(t_m)t_p] \rangle$$

Due to the straightforward relation between occupied sodium site and observed resonance frequency, lithium ions residing at the same site before and after the mixing time will lead to $\omega(0)=\omega(t_m)$, while jumps to a distinguishable site will result in $\omega(0)\neq\omega(t_m)$ and, hence, to a decay of the correlation function. This means that, in our case of disordered materials, $F_2(t_m)$ measures the probability that an ion still resides at the initial site after a time t_m. For a quantitative analysis, we need to consider that the ^{23}Na STE signal decays due to not only sodium dynamics, but also spin relaxation and spin diffusion. Specifically, following the previous approaches, we obtain $F_{SD}(t_m)$ from the ^{23}Na STE data at lower temperatures, where ion dynamics is too slow to affect the observed decays. When analysing the results at higher temperatures, we use this knowledge and fit the normalized ^{23}Na STE data to

$$F_2(t_m) = \exp\left[-\left(\frac{t_m}{\tau_k}\right)^{\beta_k}\right] \cdot F_{SD}(t_m)$$

where the first factor describes the nonexponential decay due to ion dynamics and the second factor is the fixed contribution resulting from spin diffusion. From the fit parameters τ_k and β_k, we calculate the mean logarithmic correlation time of ion dynamics.

$$ln\tau_m \equiv \langle ln\tau \rangle = \ln \tau_k + \left(1 - \frac{1}{\beta_k}\right) Eu$$

where Eu is Euler's constant (Eu=0.5772). We consider the mean logarithmic correlation time rather than the mean correlation time since, in our case of correlation functions extending over several orders of magnitude in time, the former well describes the location of the decay, whereas the latter is dominated by the long-time tail.

^{23}Na SFG diffusometry will allow us to measure self-diffusion coefficients of lithium/sodium ions. In these experiments, the resonance frequencies are determined by the positions of the spins and, thus, of the ions in the applied gradient field. Thus, ionic diffusion makes ω time dependent, leading to a decay of the STE signal according to

$$S(t_m, t_p) \propto exp\left[-(\gamma g t_p)^2 D\left(t_m + \frac{2}{3}t_p\right)\right]$$

Here, the gyromagnetic ratio γ and the field gradient g are known, leaving the self-diffusion coefficient as a single free fit parameter.

A combination of these techniques (spin-lattice relaxation (SLR), line-shape analysis (LSA), and stimulated-echo experiments (STE)) is not directly available in the groups of SIMBA partners and would require a cooperation with external research units. Furthermore, especially for ^{23}Na such experiments are not common practice and need special. Nevertheless, the efforts are planned to be undertaken to perform the described measurements on the materials investigated within SIMBA project

4 Evaluation of sodium transport via modelling

In order to model and assess the transport of sodium ion across the electrode/electrolyte interface, it is necessary first to produce the model of the electrode and electrolyte material, followed by a structural characteristic of the interface region and resistances against Na ion transport. Figure 3 shows an example of how such a material model is created for one of SIMBA anode materials, hard carbon. To create a model, first of all molecular dynamic simulation is applied, and later on the resulting structure is refined with a help of DFT calculations. In the presented examples, the modeling leads to mainly 3-fold coordinated C-network with a slight amount of 2- and 4-fold "defects".

Atomistic models of other electrode materials (Prussian White and (P2/O3) layered oxide cathode, polymer electrolyte, porous SiOC(N) anode) and those of relevant interfaces will be developed and compared with the data obtained by means of SSNMR. The verified models will then be used to further address Na diffusion channels, diffusion coefficients and contact resistances (transport across interfaces).

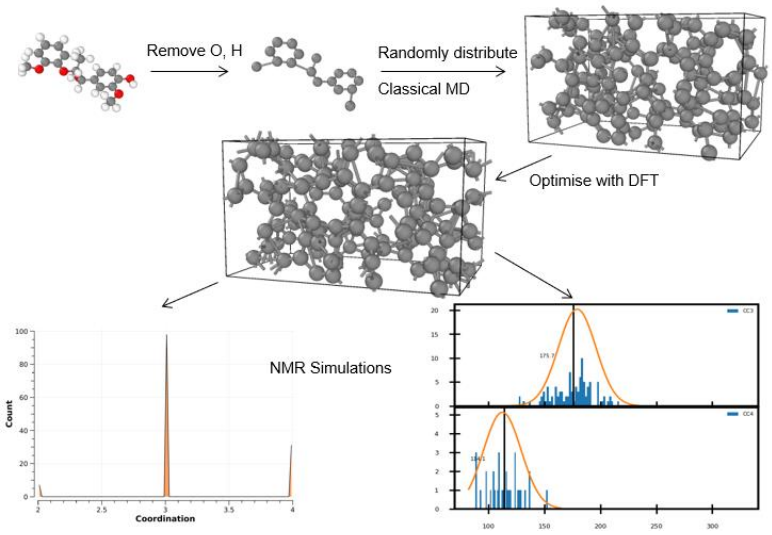

Figure 3: Single-phase disordered (hard) carbon; model construction

Nudge-elastic band methods and ab-initio molecular dynamics (ab-initio MD) will be applied on the atomistic scale to provide a comprehensive understanding of the transport phenomena. Na^+ transport will be analysed based on calculated activation barriers for Na-diffusion at electrode/electrolyte interfaces and within electrodes. While only Na^+ ions are the relevant charge carrier within the SIMBA system, the electrode-electrolyte interface also requires considering the electron transfer process. For this purpose, supercell geometries will be set up, with varying surface orientations and terminations. Since it is well known that grain boundaries in solid electrolytes are most relevant in the context of Na plating, we will also study grain boundary geometries.

In parallel, a meso-scale model based on PNP (Poisson-Nernst-Planck) equations to determine the ionic transport in the electrolyte at the interface conditions will be developed. PNP models are adapted to describe the macroscopic properties of ions transport in an electrochemical device, with links with DFT calculations. The main objective will be to adapt the PNP model to Na transport with the different interfaces.

5 Evaluation of the Na^+ transfer using single particle measurements

In order to evaluate the transport parameters of the electrode materials investigated withing SIMBA project, namely Prussian White, (P2/O3) layered oxides, porous SiCN(O) ceramics and Hard Carbon, the galvanostatic measurements using single particle measurement setup (detailed description in Deliverable 3.2) will be performed with various currents densities. Figure 4 presents an example of discharge transients recorded on the SiCN electrode. To calculate the charge transfer resistance R_{ct} and to estimate the minimum diffusion coefficient D_{min} at a depth of discharge (DOD) of 10 % the logarithm of i divided by the particles surface was plotted over the potential at 10 % DOD (Figure 4).

Nevertheless, the exact determination of $\log(i_0)$ at RT is critical and can lead to major mistakes. The reason for this is evident when having a look at the Tafel plot of SiCN-1300 at RT shown in Figure 5. The measured data points are only starting in the linear region of the Tafel plot, making it difficult to determine its onset point.

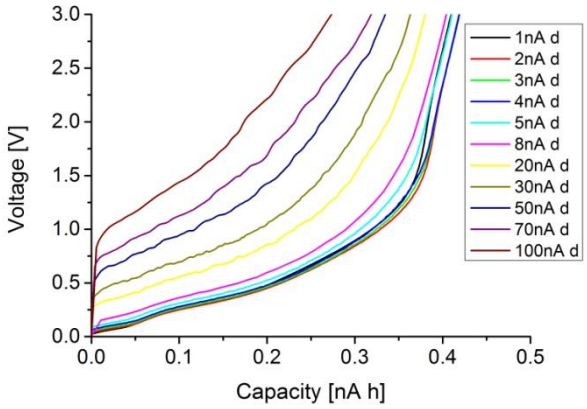

Figure 4: Rate capability for SiCN-1300 at 60 °C.

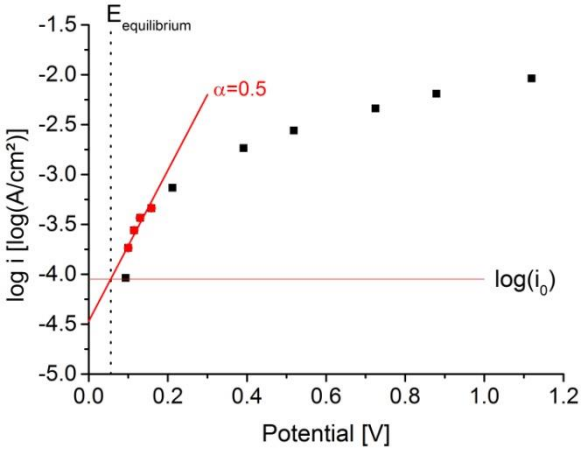

Figure 5: Tafel plot of HN3-1300 at 60 °C and DOD=10 %.

The equilibrium potential E_{equ} for a DOD of, e.g. 10 %, is taken from the mid-potential between the potential at 90 % of Depth of Charge (DOC) and 10 % of DOD during the first cycle of the rate test.

$$E_{equ} = \frac{E_{90\%DOC} + E_{10\%DOD}}{2}$$

The linear sequence of the Tafel-Plot is fitted, assuming a charge transfer coefficient of 0.5. The intercept of the linear sequence with the equilibrium potential gives rise to the exchange current density i_0. The charge transfer resistance R_{ct} will be calculated as follows:

$$R_{ct} = \frac{RT}{F \cdot i_0}$$

Moreover, the minimum diffusion coefficient D_{min} can be estimated from the linear segment of the Tafel-Plot using:

$$D_{min} = \frac{l^2}{6t}$$

The radius of the investigated particle is taken as the diffusion length l. The time t required for the Na ions to diffuse from the surface of the particle to its center is said to be the time necessary for the

complete sodiation of the particle at the last data point lying on the linear segment of the Tafel-Plot (Figure 6).

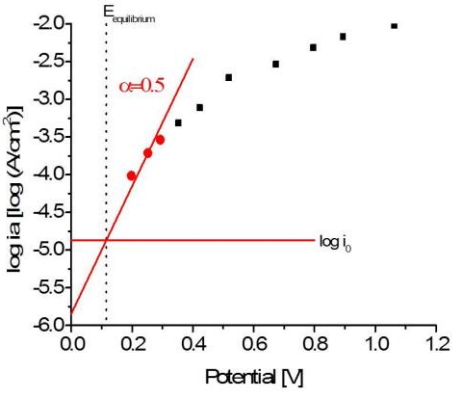

Figure 6: Tafel plot of SiCN-1300 at RT and DOD=10 %.

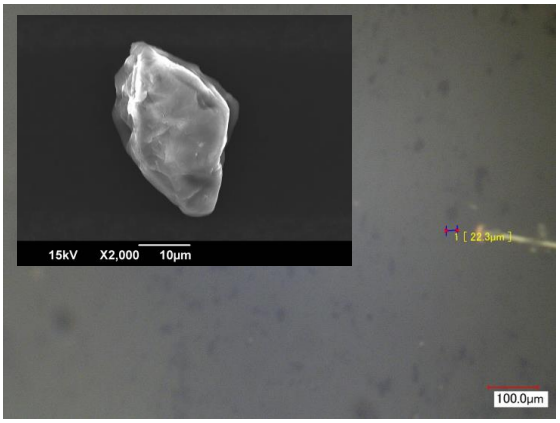

Figure 7: SEM micrograph of a single particle

Determination of the particle size used for electrochemical characterization represents a challenge and can be considered as one of the major sources of errors. For all calculations a spherical shape was assumed, however, SEM pictures reveal, that particles strongly differ in their geometry. The sufficient magnification of a particle in Figure 7 clearly shows that in some cases the particles are far from being ideally round shaped.

6 Conclusions and Recommendations

A multi-technique *in-situ* approach combining *ex-situ*/*in-situ* SSNMR and SPM techniques with theoretical modelling will allow to track the Na^+ ions in the interfacial regions. Sodium ion diffusion coefficient and charge transfer resistance will be derived experimentally by means of SSNMR and SPM and compared with values of theoretical modelling. We will integrate the knowledge of microstructure and mechanisms to model the ionic transport across the electrode-electrolyte interface. Combining experimental (SSNMR, SPM) and modelling tools will provide an in-depth understanding of interface phenomena.

An electrical model will be proposed for each material to predict the conductivity based on the composition (for the composite electrolytes) and the ionic conductivity values of the neat compounds. Theoretical models derived from the experimental results and theoretical calculations will allow to understand, predict and improve the behavior at the interfaces. As the lifetime of the battery depends strongly on the degradation mechanisms involved, the increased understanding might be applied in the algorithms for the battery management systems to maximize lifetime and safety.

7 Risk Register

Risk No.	What is the risk	Probability of risk occurrence[1]	Effect of risk[2]	Solutions to overcome the risk

[1] Probability risk will occur: 1 = high, 2 = medium, 3 = Low

[2] Effect when risk occurs: 1 = high, 2 = medium, 3 = Low

8 References

[1] M.R. Palacin, Chem. Soc. Rev., 38 (2009) 2565-2575.
[2] C. Masquelier, Nat Mater, 10 (2011) 649-650.
[3] D. Liu, W. Zhu, Z. Feng, A. Guerfi, A. Vijh, K. Zaghib, Materials Science and Engineering: B, 213 (2016) 169-176.
[4] J. Janek, W.G. Zeier, Nature Energy, 1 (2016) 16141.
[5] C. Yu, S. Ganapathy, E.R.H.v. Eck, H. Wang, S. Basak, Z. Li, M. Wagemaker, Nature Communications, 8 (2017) 1086.
[6] G. Zhonghui, S. Huabin, F. Lin, Y. Fangliang, Z. Yi, L. Wei, H. Yunhui, Advanced Materials, 30 (2018) 1705702.
[7] X. Yu, A. Manthiram, Energy & Environmental Science, 11 (2018) 527-543.
[8] Y. Tian, T. Shi, W.D. Richards, J. Li, J.C. Kim, S.-H. Bo, G. Ceder, Energy & Environmental Science, 10 (2017) 1150-1166.
[9] H.-K. Tian, Y. Qi, J. Electrochem. Soc., 164 (2017) E3512-E3521.
[10] C. Yu, S. Ganapathy, N.J.J. de Klerk, I. Roslon, E.R.H. van Eck, A.P.M. Kentgens, M. Wagemaker, J. Am. Chem. Soc., 138 (2016) 11192-11201.
[11] H. Morimoto, H. Yamashita, M. Tatsumisago, T. Minami, J. Am. Ceram. Soc., 82 (1999) 1352-1354.
[12] A. Hayashi, Y. Nishio, H. Kitaura, M. Tatsumisago, Electrochem. Commun., 10 (2008) 1860-1863.
[13] A. Hayashi, K. Noi, A. Sakuda, M. Tatsumisago, Nat Commun, 3 (2012) 856.
[14] T. Minami, A. Hayashi, M. Tatsumisago, Solid State Ionics, 177 (2006) 2715-2720.
[15] R. Böhmer, K.R. Jeffrey, M. Vogel, Prog. Nucl. Magn. Reson. Spectrosc., 50 (2007) 87-174.
[16] C. Brinkmann, S. Faske, B. Koch, M. Vogel, in: Zeitschrift für Physikalische Chemie, 2010, pp. 1535.
[17] P. Heitjans, M. Wilkening, MRS Bulletin, 34 (2009) 915-922.
[18] S. Faske, H. Eckert, M. Vogel, Physical Review B, 77 (2008) 104301.
[19] S. Faske, B. Koch, S. Murawski, R. Küchler, R. Böhmer, J. Melchior, M. Vogel, Physical Review B, 84 (2011) 024202.
[20] M. Graf, B. Kresse, A.F. Privalov, M. Vogel, Solid State Nuclear Magnetic Resonance, 51-52 (2013) 25-30.
[21] A. Kuhn, S. Dupke, M. Kunze, S. Puravankara, T. Langer, R. Pöttgen, M. Winter, H.-D. Wiemhöfer, H. Eckert, P. Heitjans, The Journal of Physical Chemistry C, 118 (2014) 28350-28360.
[22] J. Langer, V. Epp, P. Heitjans, F.A. Mautner, M. Wilkening, Phys. Rev. B, 88 (2013) 094304-094304

Appendix A - Table of Abbreviations

Symbol / Shortname	
ASSB	All-solid-state batteries
DOD	Depth of discharge
LSA	Line-shape analysis
MAS	Magic angle spinning
MD	Molecular dynamics
NMR	Nuclear magnetic resonance
PNP	Poisson-Nernst-Planck
SLR	Spin–lattice relaxation
SPM	Single particle measurement
STE	Stimulated-echo experiments

Appendix B - Acknowledgement

The author(s) would like to thank the partners in the project for their valuable comments on previous drafts and for performing the review.

Project partners:

#	Partner	Partner Full Name
1	TUDa	TECHNISCHE UNIVERSITAT DARMSTADT
2	UU	UPPSALA UNIVERSITET
3	UBham	THE UNIVERSITY OF BIRMINGHAM
4	WMG	THE UNIVERSITY OF WARWICK
5	KIT	KARLSRUHER INSTITUT FUER TECHNOLOGIE
6	CEA	COMMISSARIAT A L ENERGIE ATOMIQUE ET AUX ENERGIES ALTERNATIVES
7	IFE	INSTITUTT FOR ENERGITEKNIKK
8	SAS	USTAV ANORGANICKEJ CHEMIE SLOVENSKA AKADEMIA VIED (Institute of Inorganic Chemistry, Slovak Academy of Sciences)
9	FHG	FRAUNHOFER GESELLSCHAFT ZUR FOERDERUNG DER ANGEWANDTEN FORSCHUNG E.V.
10	JM	JOHNSON MATTHEY PLC
11	Elkem	ELKEM AS
12	YUN	YUNASKO-UKRAINE LLC
13	SAFT	SAFT
14	Altris	ALTRIS AB
15	Recupyl	TES RECUPYL SAS
16	UNR	UNIRESEARCH BV

Appendix C - Disclaimer/Acknowledgement

This project has received funding from the European Union's Horizon 2020 research and innovation programme under grant agreement No 963542. The information and views set out in this publication does not necessarily reflect the official opinion of the European Commission. Neither the European Union institutions and bodies nor any person acting on their behalf, may be held responsible for the use which may be made of the information contained therein.